APPENDIX, GSA REPOSITORY *2007045*

The Crow Wing model developed for this study had to be able to represent all aspects of

the surface and subsurface hydrologic cycle (Fig. 18).

A.1 Groundwater Flow

Time-dependent water-table fluctuations across the Crow Wing Watershed, MN are

represented by the following three-dimensional groundwater-flow equation of the

saturated zone:

$$\nabla_x \left[\overline{\overline{K}} \left(\nabla_x h \right) \right] = S_y' \frac{\partial h}{\partial t} + Q \qquad (1)$$

where

$\overline{\overline{K}}$ is the hydraulic conductivity tensor (m/s),

h is the equivalent fresh water head,

S_y' is the modified specific yield ($S_y' = S_y/b$; m^{-1}),

∇_x is the gradient operator ($\nabla_x() = \frac{\partial()}{\partial x} + \frac{\partial()}{\partial y} + \frac{\partial()}{\partial z}$),

b   is the local aquifer thickness

t is time (*s*),

Q is a source/sink term representing the rate of removal/addition of water by

evapotranspiration (ET)/infiltration (I) per unit volume of aquifer (s^{-1})

Because the Crow Wing aquifer represented in the model is unconfined, we used a modified specific yield to represent unconfined conditions (S_y', Harbaugh et al., 2000). The above equation was solved by specifying recharge along all land surface nodes with the exception of the constant-head nodes below the outlet of the watershed near the Mississippi River. Constant head boundary conditions were also applied along the sides of the solution domain directly beneath the water-table constant-head boundaries. No flow boundary conditions were imposed along the sides of the watershed in the uplands. Recharge to the aquifer across the land surface was calculated with the soil-zone model described below.

A.2 Vadose Zone

A schematic diagram illustrating the surface processes represented in our model is presented in Figure 18. For each monthly time step surface runoff was generated at each nodal patch of the triangulated surface grid. For each nodal patch (ie. area represented by each node in the triangular finite element surface mesh), a water balance calculation is performed using:

$$R = P - ET - I - \frac{\partial h_v}{\partial t} + Q_b \qquad (2)$$

where

R is the monthly runoff for a given surface node,

P   is monthly precipitation,

ET is evapotranspiration calculated as a function of monthly average temperature and vadose-zone water-balance equation (discussed below),

h_v is change in soil-moisture content represented as the change in water depth within the soil zone, and

Q_b is baseflow for nodes where the water table is at the land surface.

A.3 Runoff

Snow was converted to equivalent liquid precipitation assuming a snow density of 0.6 gm/cm^3. During winter months when the monthly temperature was below 0 ^{o}C, the snow was allowed to accumulate on the land surface. The snow is released during the first subsequent month that the mean monthly temperature exceeds freezing. The surface runoff is routed across a land-surface nodes using a DEM having a horizontal resolution of 100m. Runoff is then added to baseflow to generate total stream flow. Baseflow is evaluated for each stream node. The routing equation is given by:

$$Q_{out} = \sum_{i=1}^{N} Q_{in}^i + Q_b + R \qquad (3)$$

where

Q_{in}^i is total upstream runoff from the ith up gradient node

Q_{out} is total outflow from that node

N is the number of up gradient nodes

Note that runoff is independent of the unsaturated hydraulic conductivity of the soil and thus cannot represent extreme storm-flow events.

Baseflow (Q_b) is calculated using a form of Darcy's Law:

$$Q_b = -\frac{K^{'}}{b^{'}}[Z_{sb} - h]Lw \qquad (4)$$

where,

Z_{sb} is elevation of the stream bed,

b' is thickness of the stream bed,

$K^{'}$ is the hydraulic conductivity of the stream bed,

L   is stream segment length,

w   is stream segment width

If the water-table elevation exceeds the elevation of the top of the stream bed, baseflow is computed (gaining stream). We assumed that $K^{'}$ equals the hydraulic conductivity of the aquifer and that the stream bed depth is equal to the soil-zone thickness (2 m). If the head in the aquifer falls below the base of the stream, infiltration is calculated assuming a unit hydraulic gradient (losing stream). This amount of infiltration is then removed from the stream network ($-Q_b$). If the water table is below the stream bed and there is no upstream runoff, then the cell is treated as an upland cell.

While the approach is mass-conservative, it neglects temporal variations in stream height and stream-bank storage. Although this would be inappropriate for quantifying event-based hydrologic processes it is a reasonable assumption for quantifying long-term annual hydrologic changes. For runoff calculations, flow direction at each node is calculated based on the maximum gradient determined with the elevations of the adjacent nodes. The down-gradient node has the steepest slope among its neighboring nodes. This scheme prevents circular flow and produces a topographically based partitioning of watersheds. However, this algorithm fails to resolve situations in which a river splits into two or more branches (Renssen and Knoop, 2000). The basic assumption of our approach is that water flows downhill along the mesh segments connecting any two nodes, called flow segments. The surface mesh was designed to follow the course of major perennial streams. A topographically based routing algorithm is used to connect individual nodes into line segments starting from the upstream nodes to their final downstream nodes that constitute the stream network. This routing algorithm does not require the triangled surface mesh to be oriented in a particular direction and thus is not biased by a regular grid (Coe, 1998; Ducharne et at., 2003). While this algorithm is robust, routing problems may arise due to grid-resolution issues. For example, closed topographic depressions or "pits" can arise due to the use of a relatively coarse DEM. A pit is a topographic depression that has not many inflows, but no outflow that interrupts the stream network. A pit removal algorithm was implemented that searches for a potential downstream node within a distance of two elements and then modifies the flow direction to adjust the new flow relation to maintain the continuity of the stream network. This pit removal algorithm eliminates most of the pits but some manual adjustments are required (i.e. stream

burning; Maidment, 1996; Renssen and Knoop, 2000). These adjustments identify the incorrectly positioned streams by matching them with the actual vectorised river network and then they manually correct the mesh with the actual locations of the rivers. Of course, undrained topographic depressions containing wetlands were preserved within the model. The routing technique enables all the mesh segments potentially to be a part of a streamline, but some may be eliminated by a threshold flow below which it is not regarded as a stream segment. The model produces a dynamic flow routing network that changes its flow depending on water balance and connectivity, which depend on relative changes in water-table topography and lake levels. That is, stream segments are permitted to dry up and re-wet depending on temporal changes in local water-table elevation.

A.4 Evapotranspiration& Infiltration

Potential evapotranspiration is calculated as a function of average monthly temperature with a temperature-based equation, following Malmstrom (1969) and described in Dingman (2002):

$$e_{sat} = 6.11 \exp\left[\frac{17.3T}{237.3 + T} \right] \qquad (5)$$

$$PET = 0.00409 e_{sat} \qquad (6)$$

where

e_{sat} is the saturated vapor pressure (mbar)

T   is the monthly average air temperature (^{o}C) at grid location i for the current time step,

PET   is the monthly average potential Evapotranspiration (m/month).

Actual evapotranspiration (ET) is calculated for all surface nodes that have the water table below the root zone by multiplying potential evapotranspiration (PET) by a weighting factor (f) whose value ranges from 0 to 1, depending on the water content of the soil horizon and elevation of the water table (Fig. 19):

$$f = 1; \qquad\qquad h > Z_{soil}, h_v > h_{fc}$$

$$f = 1 + \frac{h_v - h_{fc}}{h_{fc} - h_w}; \qquad h_w < h_v < h_{fc} \qquad (7)$$

$$f = 0; \qquad\qquad h_v \le h_w$$

$$ET = f \cdot PET$$

where

f weighting factor (unitless)

h_v monthly soil moisture (m)

h monthly mean water-table elevation (m)

h_{fc} monthly field capacity of soil (m)

h_w monthly wilting point (m)

ET   monthly actual evapotranspiration (m)

PET   monthly potential evapotranspiration (m).

Z_{soil} soil base of the soil zone (i.e. land-surface minus rooting depth)

Infiltration (I) occurs when the soil-moisture content is above field capacity (h_{fc}) of the soil, the point at which the force of gravity acting on the water is greater than the surface tension, thus resulting in gravity drainage. It should be noted that the total infiltration here is assumed to recharge the aquifer, where 'recharge' is used to represent the drainage of water from the lower portion of the unsaturated soil zone into the zone of saturation. The upper limit of infiltration is restricted by the maximum saturated porosity (h_ϕ) of the soil horizon at which the excess soil moisture contributes to runoff. The lower limit of soil moisture is defined by the soil wilting point (h_w). If the water table (h) touches the base of the soil horizon (Z_{soil}), then groundwater-supported evapotranspiration at its potential rate is represented as a negative infiltration.

$$
\begin{aligned}
I &= h_\phi - h_{fc}; & h_v &> h_\phi \\
I &= h_v - h_{fc}; & h_v &> h_{fc} & (8) \\
I &= 0; & h_v &\leq h_{fc} \\
I &= -PET; & h &> Z_{soil}
\end{aligned}
$$

where

h_ϕ *soil* water volume (per square meter) at saturation expressed in terms of a water level (m)

Note that I has units of length (cm), but since monthly time steps are used its actual units are cm/month.

Actual evapotranspiration (ET) occurs at its potential value (PET) for all lake nodes and cells where the water table rises to the land surface. If the lake stage falls

below the lake bottom, the lake node is treated as a surface node and the soil-moisture balance equation is solved (eq. 5). Dry lake nodes rewet (activated) if the water table rises above the lake node bottom. At the beginning of each month, evapotranspiration, runoff, and infiltration are calculated. This approach is similar to the groundwater and surface-water algorithm implemented in MODCOU (Ledoux, et al., 1989; Ducharne et al. 2003). Here a monthly forcing of climatic parameters was chosen because the aim of this study is to assess the effects of aquifer hydrodynamics on average annual hydrologic conditions and not short term events such as floods.

A.5 Numerical Methods

The groundwater flow equation is solved using the finite element method (Zienkiewicz, 1977). Linear shape functions are used to approximate unknown heads across the tetrahedral elements. The resulting system of linear algebraic equations is solved with an indirect matrix solver (Mendoza et al. 1994). Vadose zone soil-moisture levels (h_v) in equation (11) were solved with the improved Euler's or Huen's method (Carnahan et al. 1969). Several iterations were required to calculate accurately actual soil-moisture levels and the weighting factor "f" in equation (7).

Figure DR1. Schematic diagram illustrating hydrologic processes within the land-surface model of the Crow Wing Watershed.

Figure DR2. Schematic diagram illustrating variables used in the soil-zone model.

References Cited

Carnahan, B., Luther, H.A., and Wilkes, J.O., 1969, Applied numerical methods: New York, Wiley, 604 p.

Coe, M.T., 1998, A linked global model of terrestrial hydrologic processes; simulation of modern rivers, lakes, and wetlands: Journal of Geophysical Research, D: Atmospheres, v. 103, p. 8885–8899, doi: 10.1029/98JD00347.

Dingman, S.L., 2002, Physical hydrology: New York, Macmillan, 646 p.

Ducharne, A., Golaz, C., Leblois, E., Laval, K., Polcher, J., Ledoux, E., and de Marsily, G., 2003, Development of a high resolution runoff routing model, calibration and application to assess runoff from the LMD GCM: Journal of Hydrology, v. 280, p. 207–228.

Harbaugh, A.W., Banta, E.R., Hill, M.C., and McDonald, M.G., 2000, *MODFLOW-2000*, the U.S. Geological Survey modular ground-water models; user guide to modularization concepts and the ground-water flow process: U.S. Geological Survey Open-File Report OF 00-0092, 121 p.

Ledoux, E., Girard, G., de Marsily, G., Villeneuve, J.P., and Deschenes, J., 1989, Spatially distributed modeling; conceptual approach, coupling surface water and groundwater, NATO ASI series: Mathematical and Physical Sciences, Ser. C, v. 275, p. 435–454.

Maidment, D.R., 1996, Environmental modeling within GIS, in Goodchild, M.F., et al., eds., GIS and environmental modeling; progress and research issues: [[Q22: Please give city of publication and publisher. Q22]], p. 315–323.

Malmstrom, V.H., 1969, A new approach to the classification of climate: Journal of Geography, v. 68, p. 351–357.

Mendoza, C.A., Therrien, R., and Sudicky, E.A., 1994, ORTHOFEM user's guide, version 1.02: Waterloo, Ontario, University of Waterloo, Centre for Groundwater Research.

Olcott, P.G., 1992, Ground water atlas of the United States; segment 9, Iowa, Michigan, Minnesota, and Wisconsin: U.S. Geological Survey Hydrologic Investigations Atlas Report 0730-J, p. J1–J31.

Renssen, H., and Knoop, J.M., 2000, A global river routing network for use in hydrological modeling: Journal of Hydrology, v. 230, p. 230–243, doi: 10.1016/S0022-1694(00)00178-5.

Rorabaugh, M.I., 1964, Estimating changes in bank storage and groundwater contribution to streamflow: International Association of Scientific Hydrology Publication 63, p. 432–441.

Rowntree, P.R., and Lean, J., 1994, Validation of hydrological schemes for climate models against catchment data: Journal of Hydrology, v. 155, p. 301–323, doi: 10.1016/0022-1694(94)90175-9.

Webster, K., Soranno, P.A., Baines, S.B., Kratz, T.K., Bowser, C.J., Dillon, P.J., Campbell, P., Fee, E.J., and Hecky, R.E., 2000, Structuring features of lake districts: Landscape controls on lake chemical response to drought: Freshwater Biology, v. 43, p. 499–515, doi: 10.1046/j.1365-2427.2000.00571.x.

Zienkiewicz, O.C., 1977, The finite element method in engineering science: London, McGraw-Hill, 520 p.
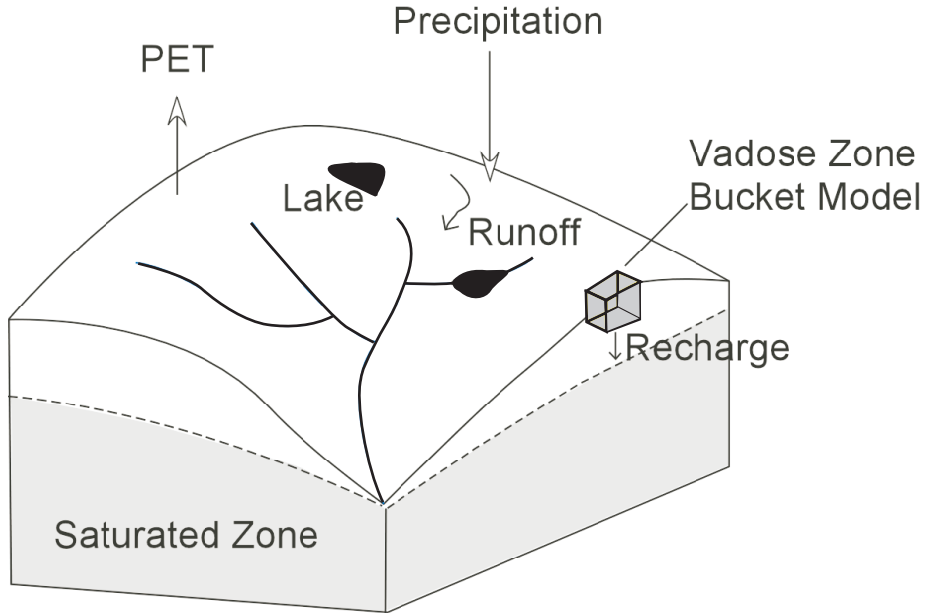
Figure 18. Schematic diagram illustrating hydrologic processes within land surface model of the Crow Wing Watershed.

Land Surface

Soil

Saturation

h_ϕ

Field
Capacity

h_{fc}

Soil
Moisture

h_v

Wilting
Point

h_w

Z_{soil}

Soil Zone
Datum = 0

Water Table

h

Hydrogeology
Datum = mean sea level